Trade winds drive pronounced seasonality in carbonate chemistry in a tropical Western Pacific island cave–Implications for speleothem paleoclimatology

Article *in* Geochemistry Geophysics Geosystems · December 2016

DOI: 10.1002/2016GC006644

8 authors, including:

Alexandra L Noronha
University of Texas at Austin
12 PUBLICATIONS **232** CITATIONS
SEE PROFILE

Jay L Banner
University of Texas at Austin
186 PUBLICATIONS **5,493** CITATIONS
SEE PROFILE

John W. Jenson
University of Guam
68 PUBLICATIONS **956** CITATIONS
SEE PROFILE

Eric James
University of Texas at Austin
45 PUBLICATIONS **776** CITATIONS
SEE PROFILE

AGU PUBLICATIONS

Geochemistry, Geophysics, Geosystems

RESEARCH ARTICLE
10.1002/2016GC006644

Key Points:
- Cave pCO_2 in tropical cave shows strong seasonality
- Trade winds contribute to flow of lower pCO_2 atmospheric air into cave
- Cave calcite deposition rate shows strong seasonality that correlates with cave pCO_2

Correspondence to:
A. L. Noronha,
anoronha@jsg.utexas.edu

Citation:
Noronha, A. L., B. F. Hardt, J. L. Banner, J. W. Jenson, J. W. Partin, E. W. James, M. A. Lander, and K. K. Bautista (2017), Trade winds drive pronounced seasonality in carbonate chemistry in a tropical Western Pacific island cave—Implications for speleothem paleoclimatology, *Geochem. Geophys. Geosyst.*, *18*, doi:10.1002/2016GC006644.

Received 12 SEP 2016
Accepted 20 DEC 2016
Accepted article online 29 DEC 2016

Trade winds drive pronounced seasonality in carbonate chemistry in a tropical Western Pacific island cave—Implications for speleothem paleoclimatology

Alexandra L. Noronha[1], Benjamin F. Hardt[1,2], Jay L. Banner[1], John W. Jenson[3], Judson W. Partin[4], Eric W. James[1], Mark A. Lander[3], and Kaylyn K. Bautista[3]

[1]Department of Geological Sciences, Jackson School of Geosciences, University of Texas at Austin, Austin, Texas, USA, [2]Department of Earth, Atmospheric, and Planetary Sciences, Massachusetts Institute of Technology, Cambridge, Massachusetts, USA, [3]Water and Environmental Research Institute of the Western Pacific, University of Guam, [4]Institute for Geophysics, Jackson School of Geosciences, University of Texas at Austin, Austin, Texas, USA

Abstract Carbon dioxide concentrations in caves are a primary driver of rates of carbonate dissolution and precipitation, exerting strong control on speleothem growth rate and geochemistry. Long-term cave monitoring studies in midlatitude caves have observed seasonal variability in cave pCO_2, whereby airflow is driven by temperature contrasts between the surface and subsurface. In tropical settings, where diurnal temperature cycles are larger than seasonal temperature cycles, it has been proposed that caves will ventilate on daily time scales, preventing cave pCO_2 from increasing substantially above atmospheric pCO_2. By contrast, the relatively small temperature difference between the surface and subsurface may be insufficient to drive complete ventilation of tropical caves. Here we present results of an 8 year cave monitoring study, including observations of cave pCO_2 and carbonate chemistry, at Jinapsan Cave, Guam (13.4°N, 144.5°E). We find that cave pCO_2 in Jinapsan Cave is both relatively high and strongly seasonal, with cave pCO_2 ranging from 500 to 5000 ppm. The seasonality of cave pCO_2 cannot be explained by temperature contrasts, instead we find evidence that seasonal trade winds drive cave ventilation and modulate cave pCO_2. Calcite deposition rates at seven drip sites in Jinapsan Cave are shown to be seasonally variable, demonstrating that speleothem growth rates in Jinapsan Cave are strongly affected by seasonal variations in cave pCO_2. These results highlight the importance that advection can have on cave ventilation processes and carbonate chemistry. Seasonality in carbonate chemistry and calcite deposition in this cave affect the interpretation of speleothem-based paleoclimate records.

1. Introduction

Accurate interpretation of speleothem-based paleoclimate reconstructions relies on understanding of the carbonate chemistry of the karst system in which speleothems form. The most fundamental example is speleothem laminae thickness, which has been demonstrated to be related to climatic and environmental variables, and is therefore frequently used as a paleoclimate proxy [*Wu et al.*, 2006; *Rasbury and Aharon*, 2006; *Rasmussen et al.*, 2006; *Tan et al.*, 2006, 2013; *Boch et al.*, 2011; *Cai et al.*, 2011; *Liu et al.*, 2013; *Van Rampelbergh et al.*, 2015; *Wong and Breecker*, 2015; *Duan et al.*, 2015; *Pu et al.*, 2015; *Riechelmann et al.*, 2016]. In addition to the value of laminae thickness as a climate proxy itself, understanding seasonal changes in the deposition rate of speleothem calcite is essential for proper interpretation of speleothem-based paleoclimate records. Seasonal changes in growth rate cause differential preservation of environmental signals, potentially biasing the paleoclimate proxy recorded by the stalagmite relative to the drip water feeding the site when sampled at annual or coarser scale [*Banner et al.*, 2007; *Baldini et al.*, 2008].

Subannual analysis of speleothems has become increasingly common through sampling of fast growing speleothems with microsampling methods [*Johnson et al.*, 2006; *Frappier et al.*, 2007; *Mattey et al.*, 2008; *Maupin et al.*, 2013; *Partin et al.*, 2013a; *Feng et al.*, 2014; *Ridley et al.*, 2015a] and use of laser ablation and secondary ionization technologies [*Wynn et al.*, 2010; *Orland et al.*, 2014; *Jamieson et al.*, 2015; *Liu et al.*, 2015]. When subannual sampling is not possible, relying on an assumption of steady growth throughout the year can lead to inaccurate interpretations of past climate [*Wong et al.*, 2011]. Additionally, there is a

growing body of evidence that demonstrates that isotope fractionation in cave calcite is related to calcite growth rate [*Watson*, 2004; *Dietzel et al*., 2009; *Feng et al*., 2012; *Gabitov et al*., 2012; *Tan et al*., 2013; *Watkins et al*., 2014; *Stoll et al*., 2015].

Understanding of the climatic and environmental controls on cave calcite deposition rates has been advanced both through experimental studies based on natural speleothem samples [*Baker et al*., 1998, 2014; *Genty et al*., 2001] or cave calcite grown on artificial substrates [*Banner et al*., 2007; *Ruan and Hu*, 2010; *Sherwin and Baldini*, 2011; *Tremaine et al*., 2011; *Wong et al*., 2011; *Casteel and Banner*, 2015; *Pu et al*., 2015], and through theoretical studies that seek to model cave calcite growth rate using principles of chemistry and physics [*Dreybrodt and Franke*, 1987; *Dreybrodt*, 1988; *Dreybrodt et al*., 1997; *Romanov et al*., 2008b]. These theoretical studies have demonstrated that the average deposition rate of stalagmite calcite (i.e., g m^{-2} s^{-1} of calcite precipitating from a drip-fed thin film in an open system with respect to CO_2) can be estimated with the equation:

$$R=\left(\left[Ca^{2+}\right]-\left[Ca^{2+}\right]_{eq}\right)\left(\frac{\delta}{t}\right)\left(1-e^{\frac{-\alpha t}{\delta}}\right) \quad (1)$$

where $[Ca^{2+}]$ is the initial concentration of calcium ions in the drip water, $[Ca^{2+}]_{eq}$ is the calcium ion concentration in equilibrium with cave pCO_2, δ is the water film thickness, t is the time interval between drips, and α is a rate constant. Water films on stalagmite surfaces are assumed to be very thin, i.e., typically $<$0.02 cm thick [*Hansen et al*., 2013], which has led workers to simplify the approximation of the term α. For a water film thickness, δ, between 0.0075 and 0.04 cm, α is independent of the film thickness, depends only on the cave temperature, T_C [*Baker et al*., 1998; *Romanov et al*., 2008a; *Hansen et al*., 2013] and can be approximated by:

$$\alpha=\left(0.52+0.04T_C+0.004{T_C}^2\right)\times 10^{-5}\ \mathrm{cm/s} \quad (2)$$

Therefore, in this model, the major controls on stalagmite calcite deposition rates are drip rate, initial drip water calcium ion concentration, cave-air pCO_2, and temperature. Drip rate and drip water calcium ion concentrations determine the delivery of Ca^{2+} to the drip site, while cave-air pCO_2 determines the degree of supersaturation of drip water after CO_2 degassing and thereby the amount of Ca^{2+} available to precipitate as calcite.

Cave monitoring studies in temperate latitudes have demonstrated distinct seasonal patterns in calcite deposition rates, which correlate with seasonal cycles in cave pCO_2 [*Banner et al*., 2007; *Baldini*, 2010; *Mattey et al*., 2010]. This result has motivated interest in cave pCO_2 variability, and has resulted in development of generalized models of cave pCO_2 and the seasonal bias of stalagmite calcite [*Baldini*, 2010; *Sánchez-Cañete et al*., 2013; *James et al*., 2015]. The primary source of high pCO_2 air in caves is biological production typically in the region above the cave [*Frisia et al*., 2011; *Breecker et al*., 2012], where pCO_2 commonly reaches values on the order of 10^4 ppm [*Atkinson*, 1977; *Benavente et al*., 2010; *Faimon et al*., 2012; *Peyraube et al*., 2013]. Production rates of this CO_2 via root respiration and microbial decomposition of organic matter are generally seasonally variable, modulated by temperature and water availability. Therefore, the pCO_2 of the cave is influenced by the biological production rate of CO_2 and the flow of both air enriched in pCO_2 and lower pCO_2 atmospheric air through the karst system.

The dominant mechanism of air flow in caves is thought to be chimney effect air flow [*Wigley and Brown*, 1976; *Covington*, 2015; *Covington and Perne*, 2015], in which flow between two entrances at different elevations is driven by density differences between cave air and outside air. *Covington* [2015] recently demonstrated through dimensional analysis that these "entrances" need not be the human-sized openings traditionally thought of as entrances. In fact, these cave openings need only be 1 mm in diameter with an elevation difference of 30 cm—conditions that are present in most caves that are the sites of paleoclimate research, in the form of fractures and conduits in the karst. The density differences that drive chimney effect air flow are caused largely by temperature contrasts between the surface and subsurface. Because cave temperatures tend to be relatively constant year round, and approximate the local annual average surface temperature, changes in surface temperature are the main driver of changes in the temperature contrast between the surface and the subsurface. In the example of a cave with a large lower entrance situated below the epikarst and vadose zone, when surface temperatures are warmer than the subsurface, cave air is dense relative to surface air and will flow out the lower entrance, pulling in air enriched in CO_2 from the

vadose zone above and surrounding the cave. By contrast, when surface temperatures are lower than the subsurface, cave air buoyantly rises, reversing the direction of flow and the cave fills with lower pCO_2 atmospheric air.

James et al. [2015] suggested that in tropical regions, which have a more muted seasonal temperature regime than the midlatitudes, caves will ventilate daily, potentially preventing pCO_2 from ever reaching levels that would inhibit calcite growth. However, the velocity of air flow is proportional to the temperature differences between the surface and subsurface [*Covington*, 2015]. Therefore, alternatively, it may be expected that the daily temperature contrasts in the tropics are insufficiently large to drive complete ventilation of caves. Here we report the results of 8 years of detailed monitoring of drip water, pCO_2, and calcite deposition rates in a tropical cave to investigate the controls on tropical cave pCO_2 and stalagmite calcite deposition rates.

2. Materials and Methods

2.1. Site Description

The United States Territory of Guam (13.4°N, 144.5°E) is the largest and southernmost island in the Mariana Island volcanic island arc. Guam lies in the northern region of the West Pacific Warm Pool, and receives 2000–2500 mm of rainfall annually over distinct wet and dry seasons, with ∼70% of annual precipitation occurring during the July–December wet season [*Lander and Guard*, 2003]. This seasonality in rainfall, as well as seasonality in surface winds, is related to the migration of the Intertropical Convergence Zone (ITCZ; Figure 1). During the dry season, the position of maximum precipitation is located south of the island and persistent northeasterly trade winds blow across the island. During the dry season, most rain falls as light showers. The wet season is driven by expansion of the monsoon trough and the northerly shift of the position of maximum precipitation. During this season, the trade winds slacken and typically shift southeastward, resulting in more humid and unstable atmospheric conditions over the island. Formation of convective clouds drives moderate to heavy downpours, which are responsible for the majority of wet season precipitation [*Lander et al*., 2001]. Wet season precipitation is also affected by tropical cyclone activity, with ∼30% of Guam's wet season precipitation induced by tropical cyclones [*Kubota and Wang*, 2009]. Mean daily temperature is 27.4°C with a seasonality of <2°C, while the diurnal temperature range is ∼4°C (Figure 2).

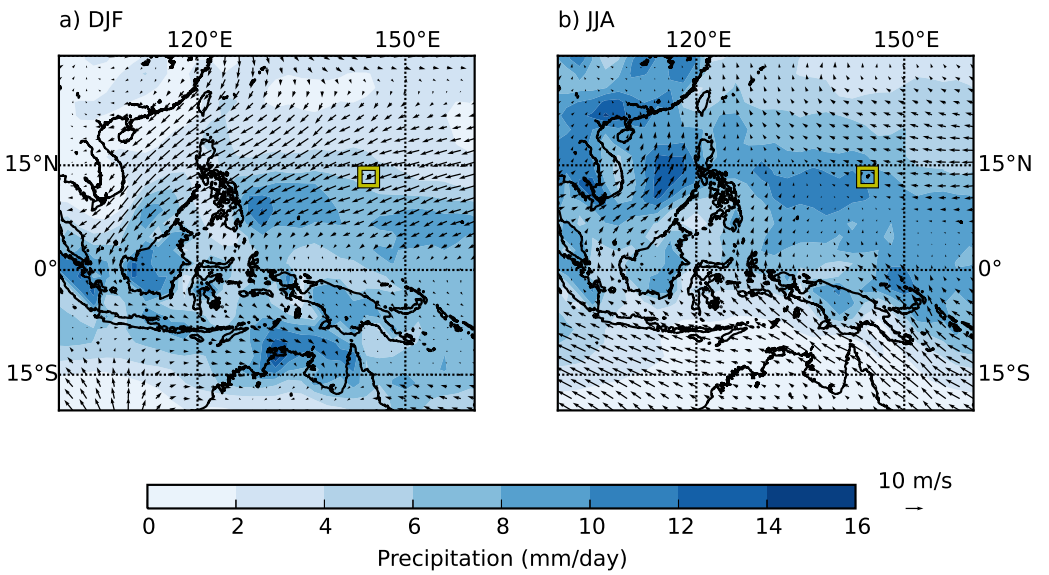

Figure 1. Long-term mean wind (vectors) [*Kalnay et al*., 1996] and precipitation(shading) [*Xie and Arkin*, 1996] in the western tropical Pacific Ocean during (a) the boreal winter and (b) summer. Climate data obtained from NOAA/ESRL Physical Sciences Division, Boulder Colorado (esrl.noaa.gov/psd). Position of the island of Guam is highlighted with a yellow square.

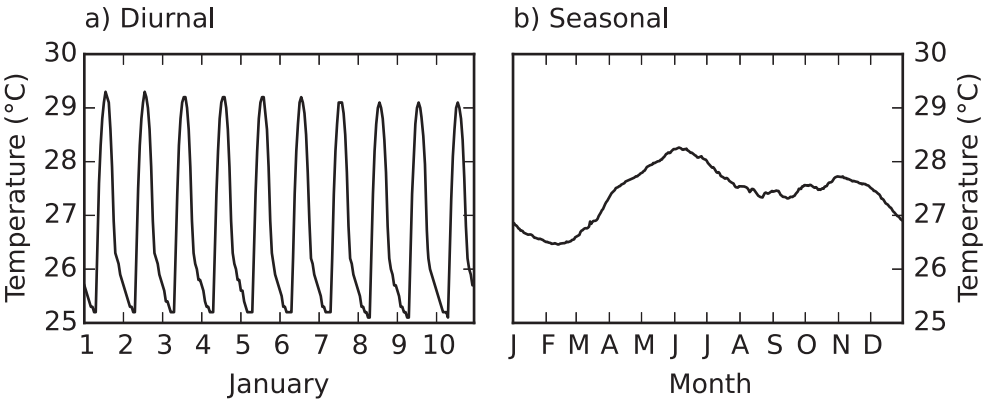

Figure 2. (a) Hourly average air temperature normals for the first 11 days of January illustrating the ~4°C diurnal temperature cycle, and (b) daily average air temperature normals spanning the whole year illustrating the <2°C seasonal temperature cycle at the Guam International Airport (GHCND:GQW00041415). Climate normals obtained from NOAA CDO.

The northern half of the island is comprised of an uplifted carbonate plateau containing numerous caves. Jinapsan Cave is a progradational collapse cave [*Miklavič*, 2011] located on the northernmost point of the island, near Ritidian Point (Figure 3). The cave is located within 500 m of the beach in limestone forest, at the base of the cliff line, beneath a vegetated talus wedge. The ~1 m diameter cave entrance is eastward facing. The cave is composed of a single chamber, though large flowstone deposits and stalagmites partially partition the chamber into multiple rooms (Figure 4). At the base of the cave is a brackish water table pool which exhibits a strong hydraulic connection to the ocean tide.

2.2. Cave and Weather Monitoring

Sampling of cave drip water at Jinapsan Cave began in early 2008, and a routine monthly collection program was undertaken August 2008 to September 2016. Samples were collected at seven drip sites and the cave pool [*Partin et al*., 2012]. The work presented in this paper considers samples from the drip sites named Flatman, Station 1, Station 2, Stumpy, Stumpy's Brother, Amidala, and Trinity. Station 2 is the site of a

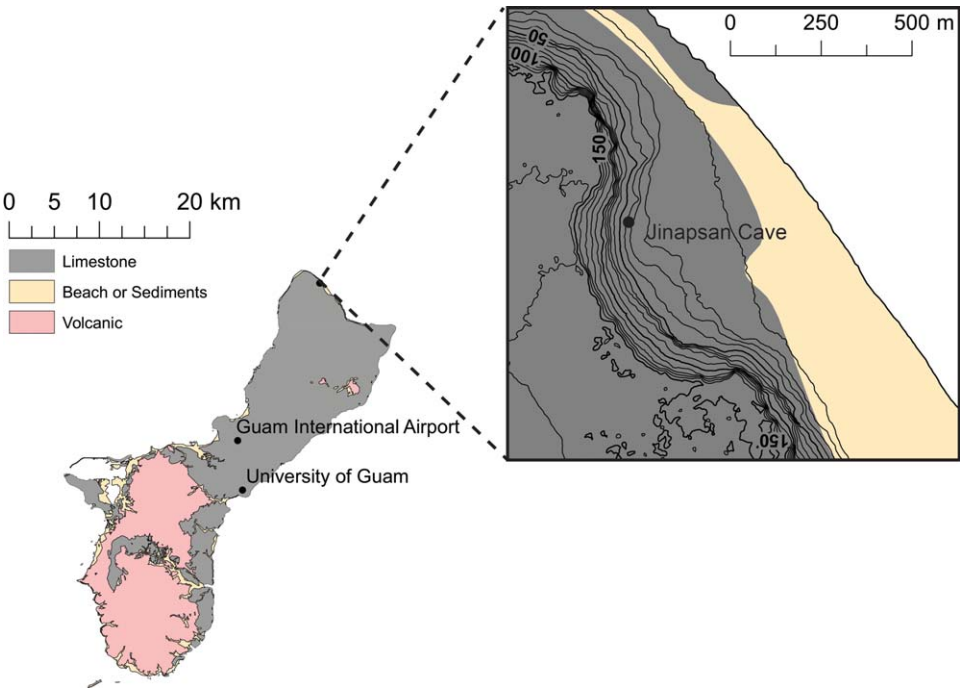

Figure 3. Island of Guam with close-up of location of Jinpansan Cave in base of cliff ~500 m from coastline.

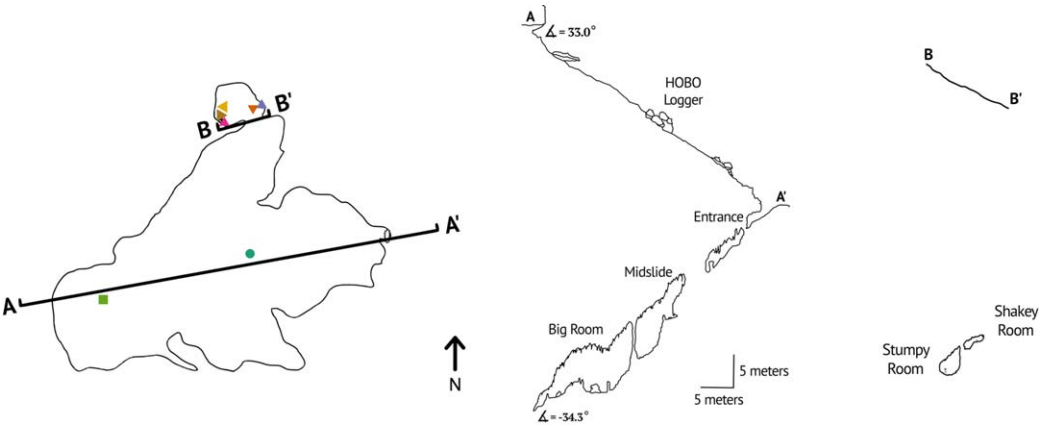

Figure 4. Plan view of perimeter of Jinapsan Cave, with cross sections. Colored markers show positions of drip sites.

stalagmite referred to as "Big Guam" or "Shakey," from which paleoclimate results have been previously been reported [*Sinclair et al*., 2012]. Paleoclimate results from the stalagmite, Stumpy, were reported by *Partin et al*. [2012]. The monthly monitoring program included collection of water samples and drip-rate data, collection of calcite precipitated onto glass plates, and rotation of instruments that log cave-air pCO_2, temperature, barometric pressure, and relative humidity.

Drip water was collected in preweighed wide-mouthed HDPE Nalgene bottles that were deployed under the drips for ~24 h. Collection bottles were weighed and water was decanted in the cave into bottles and pretreated for a suite of geochemical analyses. Aliquots of drip water for analysis of cation concentrations are stored in acid-washed 30 mL HDPE Nalgene bottles and preserved with 60 μL of Seastar nitric acid. When sufficient water remained after aliquots had been decanted, pH, conductivity, and water temperature were measured in the cave using a Myron Ultrameter II-6P (Myron L Company, Carlsbad, CA, USA).

Drip rates were measured manually with a chronometer. Standard protocol was to measure the interval between three consecutive drips three times and report the average of these measurements as the drip interval. When the drip interval was >300 s the long drip interval was noted, but no measurement of drip interval was taken. When drip interval was especially short, typically <10 s, the total number of drips in 3 min was counted. In this manuscript, in cases where measured drip interval is unavailable, drip interval is estimated from the mass of water collected, using a density of 1.0 g/mL, and assuming a constant drip volume for each site. Site-specific drip volumes are obtained as the average of the drip volume calculated from recorded measurements of sample mass and drip intervals.

Calcite was accumulated on 10 cm × 10 cm glass plates on which the surface had been frosted to facilitate calcite nucleation. Plates were placed under active drips for 3–12 weeks. In January 2012, permanent plate holders made of PVC pipe were installed under each drip site to insure consistent plate orientation. Plates were engraved with an identifier on the smooth side, and placed in the holder so that the left-hand corner faced northeast. Plates were deployed with a slight incline, and dip directions of the plates were noted. To determine calcite growth rate, each plate was weighed with a Sartorius MCI RC 210P electronic balance (Sartorius, Goettingen, Germany) before deployment in the cave and after recovery from the cave. A standard plate was weighed to reduce variability in plate weight measurements associated with static electricity, humidity, etc., following methods established by *Banner et al*. [2007]. Long-term variability in standard plate weight measurements is ~0.5 mg.

Data loggers deployed both in and outside of the cave were collected monthly. For all stations where data loggers were deployed, there were at least two instruments dedicated to the site that were deployed in alternate. A HOBO Micro Station Data Logger was deployed on the talus slope above the cave logging air temperature and pressure. Logging resolution ranged from 1 min to 1 h, with most recent measurements at 1 h intervals.

Cave pCO_2 was logged in low-power mode at 1 h intervals using a Vaisala GM70 CO_2 probe (0–5000 ppm calibrated measurement range) and Vaisala M170 data logger (Vaisala Corp, Helsinki, Finland), deployed in

the Stumpy room. Spot check measurements of pCO_2 were taken with a separate logger in the Shakey Room, at Midslide and the Big Room during most field trips. Beginning in 2012 the CO_2 logging assembly was deployed with the probe extending from a sealed orifice in a Pelican dry box (Pelican Products, Inc., Torrance, CA, USA) containing ~500 g of desiccant (Drierite desiccant (W.A. Hammond Drierite Co. Ltd., Xenia, OH, USA) or generic vermiculite). Cave-air temperature, pressure, and relative humidity were logged at 1 h intervals using HOBO Micro Station Data Loggers (HOBO, Onset, Bourne, MA, USA).

2.3. Elemental Analysis

Major ion concentrations were determined in facilities in the Department of Geological Sciences at the University of Texas at Austin (UTA) using an Optima 4300 inductively coupled plasma optical emission spectrometer (ICP-OES) or an Agilent 7500ce quadrupole ICP-mass spectrometer (ICP-MS). Drifts in emission response on the ICP-OES over the course of the run were corrected for by running a reference standard of known concentration, along with two matrix standards, after every fifth sample, modified after the protocols of *Schrag*, [1999]. Multiple emission lines were measured for each analyte. Reported values reflect the most precise and accurate measurement for the given analyte during the sample run. Reference standard measurements were within 2.5% (2σ) of known gravimetric concentrations with relative standard deviations of 4% or less. Reference concentrations used in ICP-OES analyses were independently verified by ICP-MS. Samples analyzed on the ICP-MS were diluted 1:10 with 2% HNO_3. Machine drift was compensated for by mixing with an internal standard solution of ^{45}Sc, ^{89}Y, ^{165}Ho, and ^{169}Tm. Analytical uncertainty, determined by the RSD of replicate measurements of NIST 1643e, was $\leq$4% for elements reported in this manuscript. Procedural blanks were indistinguishable from reagent blanks.

2.4. Models of Cave Ventilation and Calcite Deposition

The predicted direction of air flow within the cave is modeled simply by the hourly temperature difference between the surface and subsurface using observed temperature. To compensate for missing data, we create synthetic annual compilations at hourly resolution of both the subsurface and surface temperature based on the observed measurements. Daily average subsurface temperature is modeled by averaging all logged cave temperature data for each calendar day and interpolating cave temperature hourly using a locally weighted scatterplot smoothing function. The surface temperature compilation is the average of all measurements taken during the same hour of each year over the period of logging. We compare the modeled surface and subsurface temperature series hourly and sum the hours of the day during which the temperature contrast predicts flow in and out of the human-sized cave entrance. A composite time series of cave pCO_2 is also constructed by taking the average of all logged data for each calendar day.

The growth rate model as described above (equations (1) and (2)) was implemented in a Python script. Calcite deposition rates are calculated for all drip water samples that have been analyzed for $[Ca^{2+}]$ ($n = 366$). When reliable cave pCO_2 measurements are available, the average of all cave pCO_2 measurements logged during the field trip is used. In cases where logged cave pCO_2 is unavailable, pCO_2 is assumed to be 4500 ppm July–November and 500 ppm otherwise, based on rounding of the average observed high and low season values (Figure 9). Equilibrium $[Ca^{2+}]$ is calculated in the script using PHREEQC via the phreeqpy package.

Water temperature, T, is held constant at 26.5°C and film thickness, δ, is assumed constant for all calculations at 0.01 cm. The area of deposition and total mass of calcite expected to be deposited on the glass plate is calculated from the thin film thickness and the drop volume. When drip interval and drip mass were both measured at a site during the same field trip, the drip volume is calculated directly, otherwise the average of all calculated drip volumes for the site is used as described above.

3. Results

3.1. CO_2 and Temperature Time Series

Average recorded temperature in Jinapsan Cave temperature is 25.9 ± 0.1°C, which is 0.5°C lower than the contemporaneous annual average of the temperature logged above the cave (26.4 ± 1.1°C; Figure 5).

A clear difference is observable in measured cave pCO_2 between data collected before and after the field trip on 26–27 March 2012 when desiccant was added to the dry box enclosing the data logger, as standard procedure. Before routine use of desiccant, instrument failure was more common and negative pCO_2 values

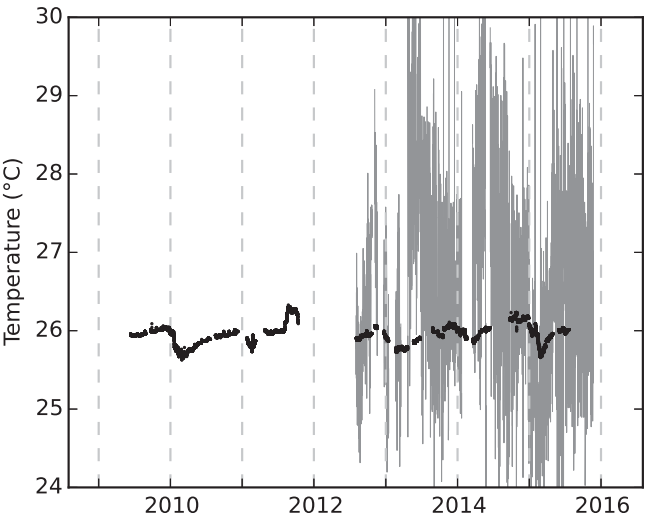

Figure 5. Temperature recorded in Jinapsan Cave (black line) and on the hill slope above the cave (grey line).

were recorded frequently. Because of these data-quality issues, we do not consider measured cave pCO_2 before 27 March 2012 reliable data. Measured cave pCO_2 from 27 March 2012 onward shows a clear seasonal cycle, with high and variable seasonal average pCO_2 values of 2500 ± 1500 ppm observed during July–December wet season and low and more stable average pCO_2 of 570 ± 160 ppm observed during January–June dry season. Spot check measurements showed pCO_2 in the Shakey Room and Big Room were identical within instrument precision, while pCO_2 at Midslide follows the seasonality of the other sites, but has a maximum value of 1900 ppm.

3.2. Cave Drips

Drip rates at the seven sites range from periods of complete cessation of dripping to as many as 200 drips/min (Figure 6). Except for the two sites with the lowest drip rates, Stumpy and Amidala, drip rates at all drip sites show a clear response to precipitation infiltration, with sharp increases in drip rates following the first large wet season storm event. Drip rate at Station 2 displays this seasonality, and overall drip rate has been progressively decreasing over the period of monitoring, from a maximum of 2 drips/min in August 2008 to 0.6 drips/min in November 2015. Amidala has the lowest average drip rate, although it occasionally displays intervals of higher drip rates that do not correspond to the same storms that appear to drive seasonal increases in drip rate at other sites. Trinity has the highest drip rates, with all observed drip rates >38 drips/min.

Drip water temperature was measured only when sufficient water remains following collection for geochemical analysis, resulting in a bias in measurements toward the fastest drip rate sites. The average drip water temperature of 26.5 ± 0.6°C is slightly higher than the contemporaneous cave-air temperature (25.9 ± 0.1°C).

Calcium ion concentrations measured in drip waters collected at three Jinapsan Cave sites—Flatman, Stumpy's Brother, Station 2—are higher and less variable than $[Ca^{2+}]$ at the four other Jinapsan Cave sites—Amidala, Station 1, Stumpy, and Trinity (Figure 7). In the latter three sites, a seasonal cycle is evident, which broadly follows the seasonality in cave pCO_2.

3.3. Calcite Deposition

All glass plates deployed under drips have some visible calcite growth, although for some glass plate samples, recorded weights following collection are lower than recorded weights before deployment, suggesting chipping or plate erosion may be occurring. In Figure 8, plates with negative growth rates are shown as 0 mg/d deposition rates. There is a clear seasonality in calcite deposition rate at Stumpy, Stumpy's Brother, and Station 2 while Flatman, Amidala, and Trinity do not exhibit seasonality in deposition rate. Both Trinity and Amidala, the fastest and slowest dripping sites, respectively, rarely have appreciable calcite deposition. Intervals for which Amidala has appreciable calcite growth correspond to intervals where drip rate increased.

Calcite deposition rates predicted by the stalagmite calcite deposition rate model employed here are shown in the dashed lines and open symbols in Figure 8. In the time series view, the agreement between the modeled and measured data appears to be poor. The model as applied here consistently underpredicts deposition rate at Flatman, while it overpredicts growth rate at Stumpy and Trinity.

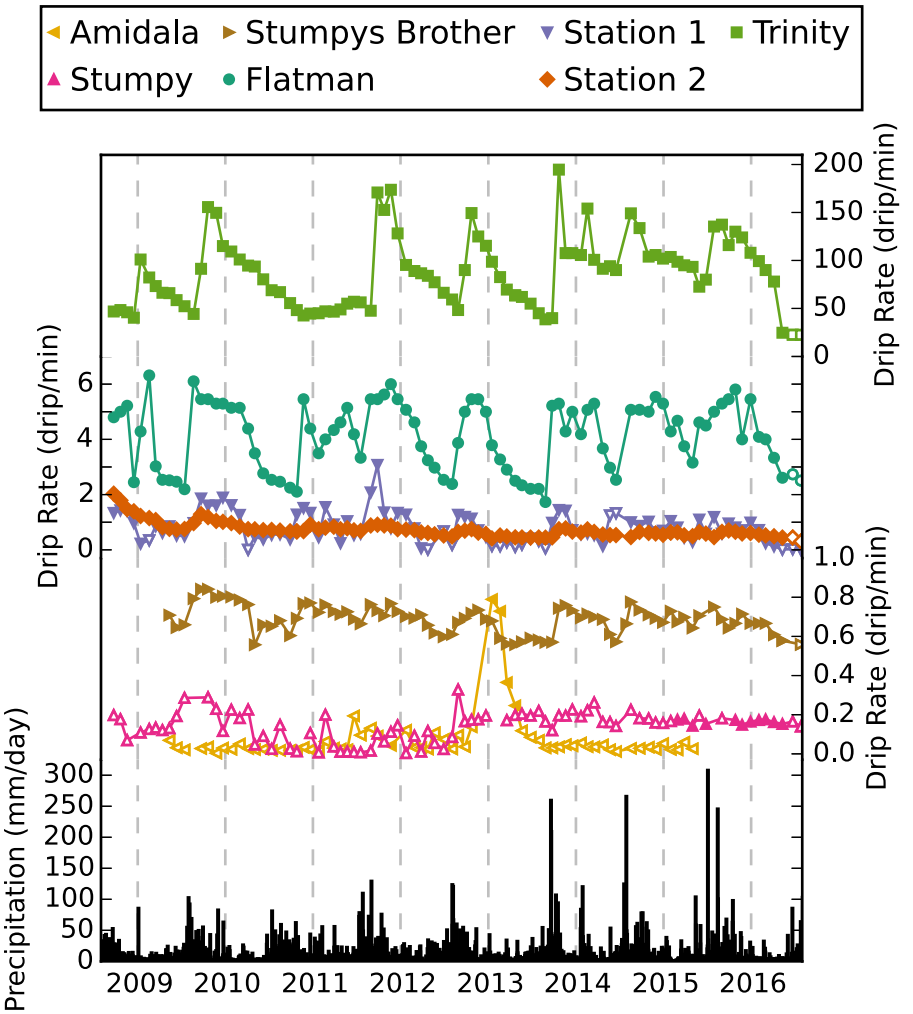

Figure 6. Daily precipitation amount at the Guam International Airport (GHCND:GQW00041415) and Jinapsan Cave drip rate. Drip rate at all seven drip sites in three subplots by increasing drip rate. Filled symbols denote values that were measured by chronometer, open symbols denote values that were calculated from the collected volume assuming a constant drip volume. Precipitation data obtained from NOAA CDO (ncdc.noaa.gov/CDO).

4. Discussion

4.1. Cave Ventilation

Seasonality in cave pCO_2 can be affected by a combination of changes in both the rate of biogenic CO_2 production and cave ventilation, but at Jinapsan Cave it is reasonable to rule out changing production rate as an important driver of the observed cave pCO_2 seasonality. In general, it is unlikely that seasonal soil and epikarst CO_2 production rates in a tropical site ever decrease so low as to drive a decrease in pCO_2 to the near-atmospheric concentrations (~500 ppm) we observe in the cave during the low pCO_2 season [*Malhi et al.*, 1999; *Mcgroddy and Silver*, 2000]. More specific to Guam, *Motavalli et al.* [2000] monitored soil CO_2 efflux rates at a forest site located on Andersen Air Force Base, <5 km south of Jinapsan Cave, from October 1996 to September 1997. During this period, Guam experienced both large typhoons and drought conditions, but soil CO_2 efflux rates in the forested site remained relatively constant at ~10 μmol/m^2 s. Based on these observations, we argue cave ventilation must be the primary mechanism driving seasonality in Jinapsan Cave pCO_2.

Using a composite time series of our observations of temperature in the surface and subsurface as described in section 2.4, we consider evidence for chimney effect air flow in Jinapsan Cave. Figure 9 shows the percentage hours of each calendar day when cave temperature exceeds surface temperature (blue) and vice versa (orange). When cave temperatures are higher than surface temperatures, chimney-effect air flow

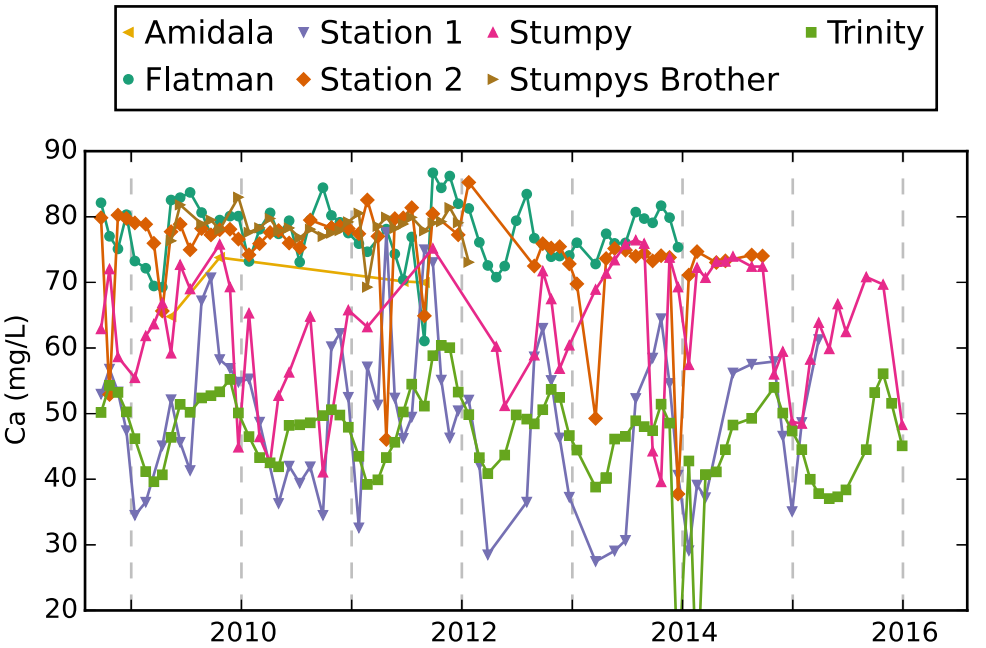

Figure 7. Drip water [Ca^{2+}] measured at seven Jinapsan Cave sites.

should be expected to pull low-pCO_2 air into the cave through the human-sized entrance. When cave temperatures are lower than surface temperatures air flow out of the cave entrance should be expected to pull high-pCO_2 air down into the cave. Cave pCO_2 in Jinapsan Cave (black line) shows strong seasonality, with low concentration in the dry season and high concentrations in the wet season.

There is some correspondence between the flow direction predicted by the surface/subsurface temperature differences and measured cave pCO_2. High pCO_2 only occurs during the wet season when the temperature contrast predicts air flow will draw high-pCO_2 air into the cave, while low pCO_2 occurs primarily during the dry season when low-pCO_2 air should flow into the cave. However, there is a period of the year—from April to mid-June—where temperature contrasts predict strong inflow of high-pCO_2 air into the cave, but

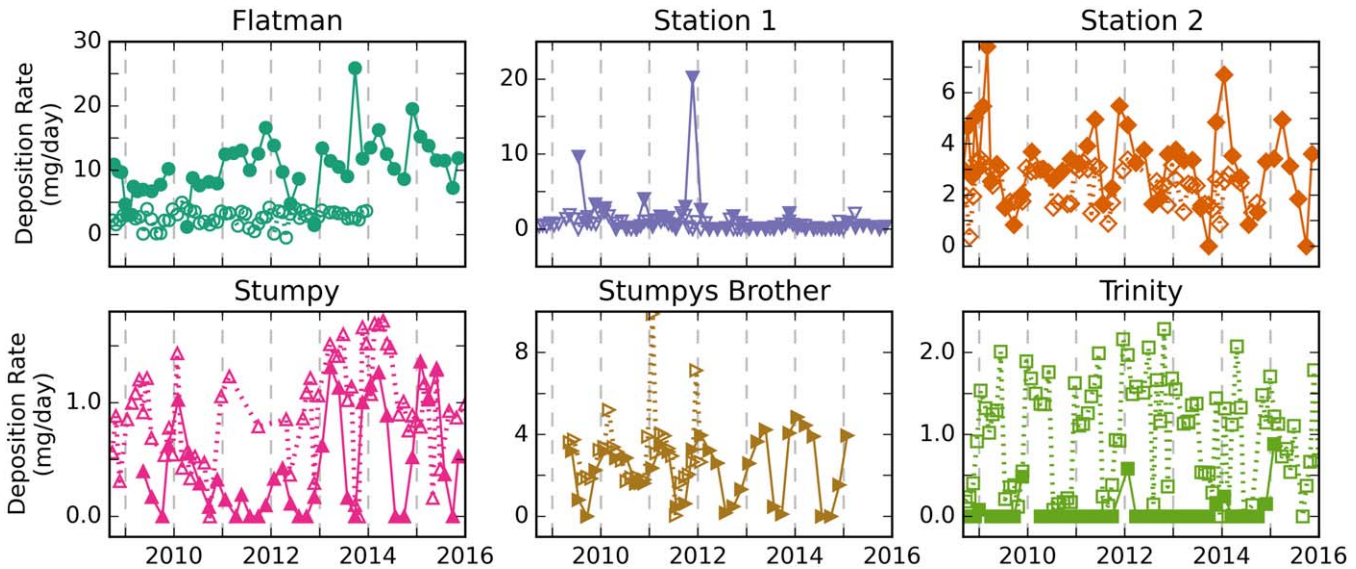

Figure 8. Measured (filled symbols) and modeled (open symbols) calcite deposition rate at all sites. Note the variable *y* axis ranges. Calcite depisiton rate is not modeled for Amidala because low drip rates do not yield sufficent water for [Ca^{2+}] measurements.

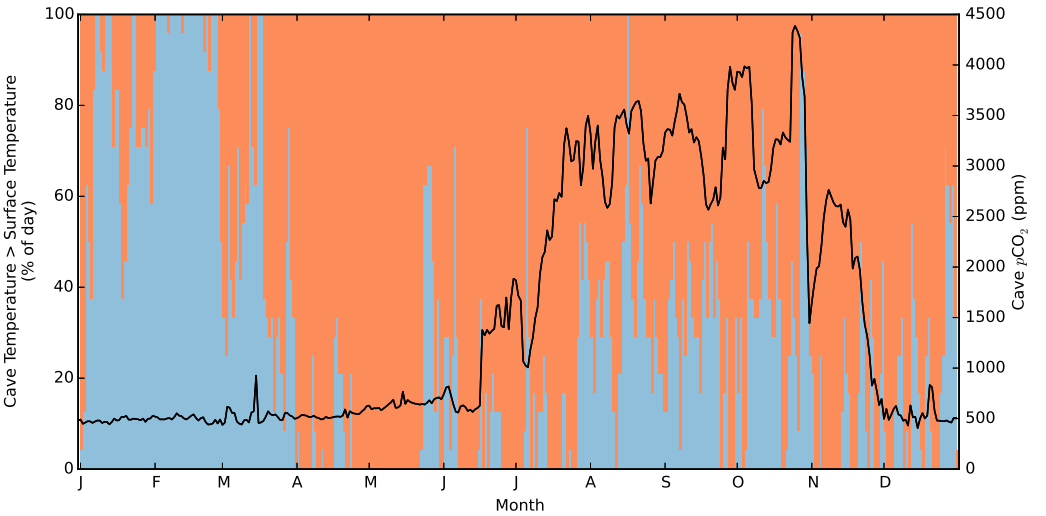

Figure 9. Temperture contrast between the surface and subsurface at Jinapsan Cave based on composite of logged temperatures and pCO_2. Blue region is percentage of the day when cave temperature is higher than surface temperature, and therefore low pCO_2 external air should flow into the cave through the entrance. Orange region is percentage of the day when cave temperature is lower than surface temperature and therefore air should move the opposite direction, bringing high pCO_2 air into the cave. Black solid line is daily average cave pCO_2 over the period of observation.

observed cave pCO_2 is near atmospheric values. These patterns suggest that while chimney effect air flow may be occurring at Jinapsan Cave, ventilation driven by temperature contrasts between the surface and subsurface alone is insufficient to explain the all of the observed seasonality in cave pCO_2.

The rapid drop in cave-air pCO_2 coincides with the onset of the dry and windy season, suggesting that the seasonal trade winds may ventilate the cave. In Figure 10, we compare the seasonal pattern of cave pCO_2 to the temporal pattern of the trade winds. We define the trade winds here as winds with speed $>$5 m/s and direction from between 0° and 180°. The strong correspondence between the rapid rise and fall in cave pCO_2 and the annual termination and onset of the trade wind strength, respectively, suggests that the trade wind flow across the island exerts strong control on cave pCO_2 in Jinapsan Cave. This effect is further illustrated in Figure 11. In this figure, it is evident that cave pCO_2 is lower when winds originate from

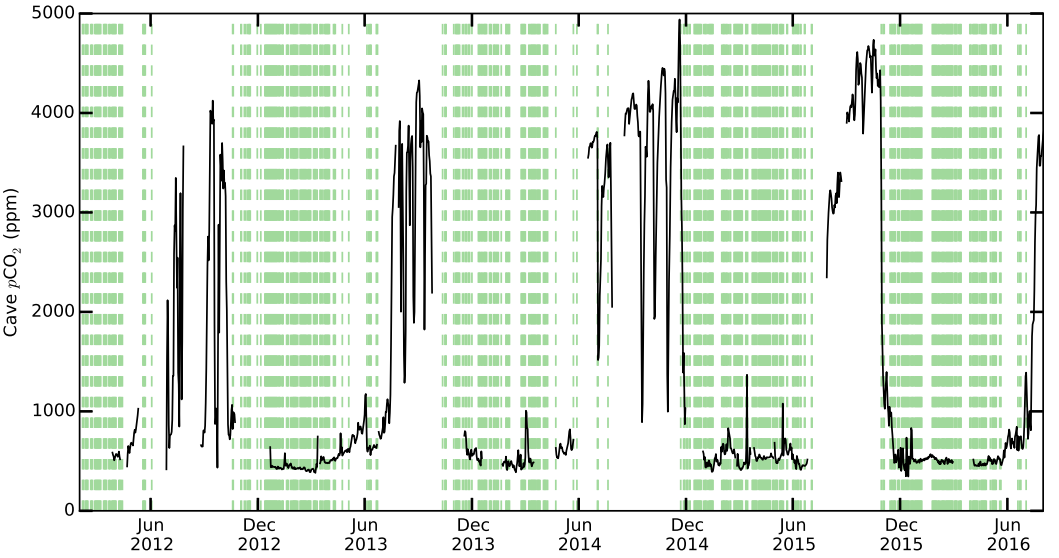

Figure 10. Cave pCO_2 (black solid line) observed at Jinapsan Cave and days during which the speed of the daily fastest 2 min winds at the Guam International Airport (GHCND:GQW00041415) is $>$5 m/s and originates from 0°–180° (dashed green vertical lines). Daily wind data obtained from the National Climatic Data Center [*Menne et al.*, 2012].

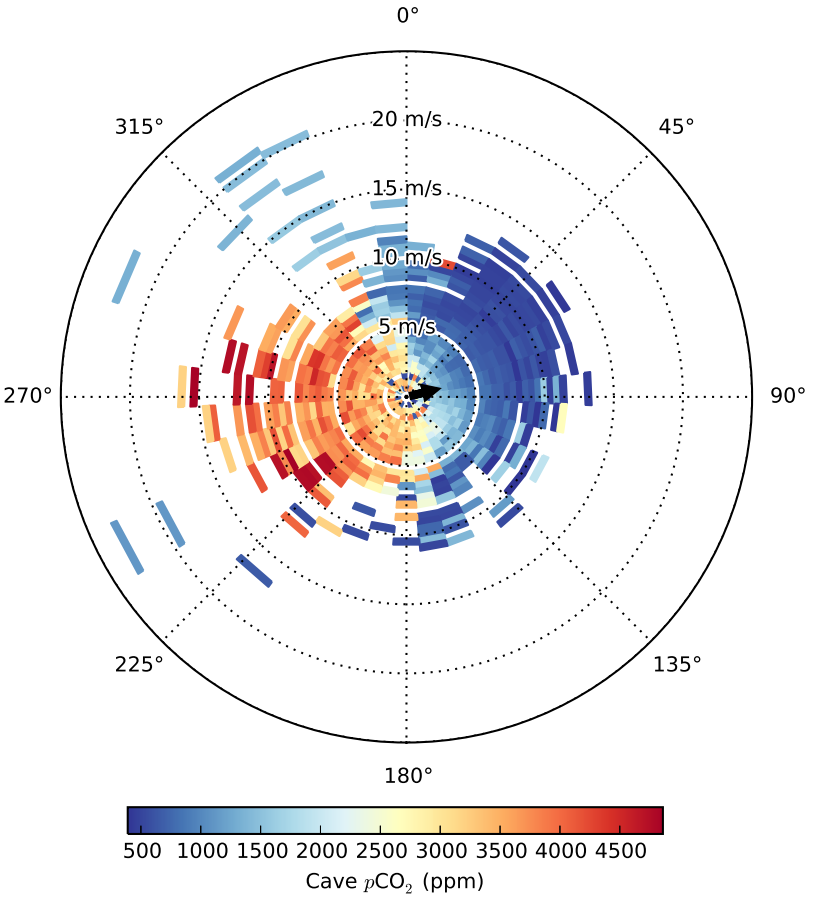

Figure 11. Polar plot of average cave pCO_2 (color bar) versus wind direction (theta) and wind speed (radius). Black arrow points perpendicular to the direction of Jinapsan Cave's human-sized entrance. Guam International Airport (USAF: 912120) hourly wind data obtained from the National Climatic Data Center Integrated Surface Data [*Smith et al.*, 2011].

~0° to 180° and higher when winds originate from ~180° to 360°. Cave pCO_2 decreases with increasing wind velocity for winds originating from 0° to 180°, and when winds originate from 180° to 360° and speeds are >15 m/s. These patterns suggest that the cave is ventilated by winds that blow into or orthogonal to the cave entrance, and that the cave's location in a cliff face shields the cave from all but the strongest winds coming from other directions.

Cave pCO_2 values of 5000 ppm have been observed at Jinapsan Cave, which appears to be an especially high value relative to published results for the tropics. To our knowledge, tropical cave pCO_2 has only been reported previously four times in the literature. The two published time series of cave pCO_2 at tropical cave sites—from Yok Balum Cave, Belize (16.2°N, 89.1°W) [*Ridley et al.*, 2015b] and Niue Cave, Niue Island (19.1°S, 169.9°W) [*Tremaine et al.*, 2016]—show pCO_2 varying seasonally between near ambient pCO_2 and ~800 ppm. Spot measurements made in several caves across Boreno in June 2006 never exceeded 800 ppm [*Partin et al.*, 2013b], and a range of 1180–2720 ppm measured during five field trips at unspecified times during a 15 month period was reported at São Bernardo Cave, Brazil (13.8°S, 46.4°W) [*Moquet et al.*, 2016]. Within this small set of published tropical cave pCO_2 measurements, Jinapsan Cave pCO_2 has the largest amplitude seasonal cycle.

4.2. Carbonate Chemistry Controls on Calcite Deposition Rates

Seasonality in cave pCO_2 at Jinapsan Cave drives seasonality in carbonate chemistry of the system, which is evident here in changes of the rate of speleothem deposition. Changes in pCO_2 of the system drive changes in both the equilibrium $[Ca^{2+}]_{eq}$ and initial drip water $[Ca^{2+}]$. While we have not measured pCO_2 at other depths at our study site, a recently published study by *Sánchez-Cañete et al.* [2016] demonstrated influence of wind-driven ventilation on soil and epikarst pCO_2. Lower pCO_2 in the zone of calcite dissolution will act

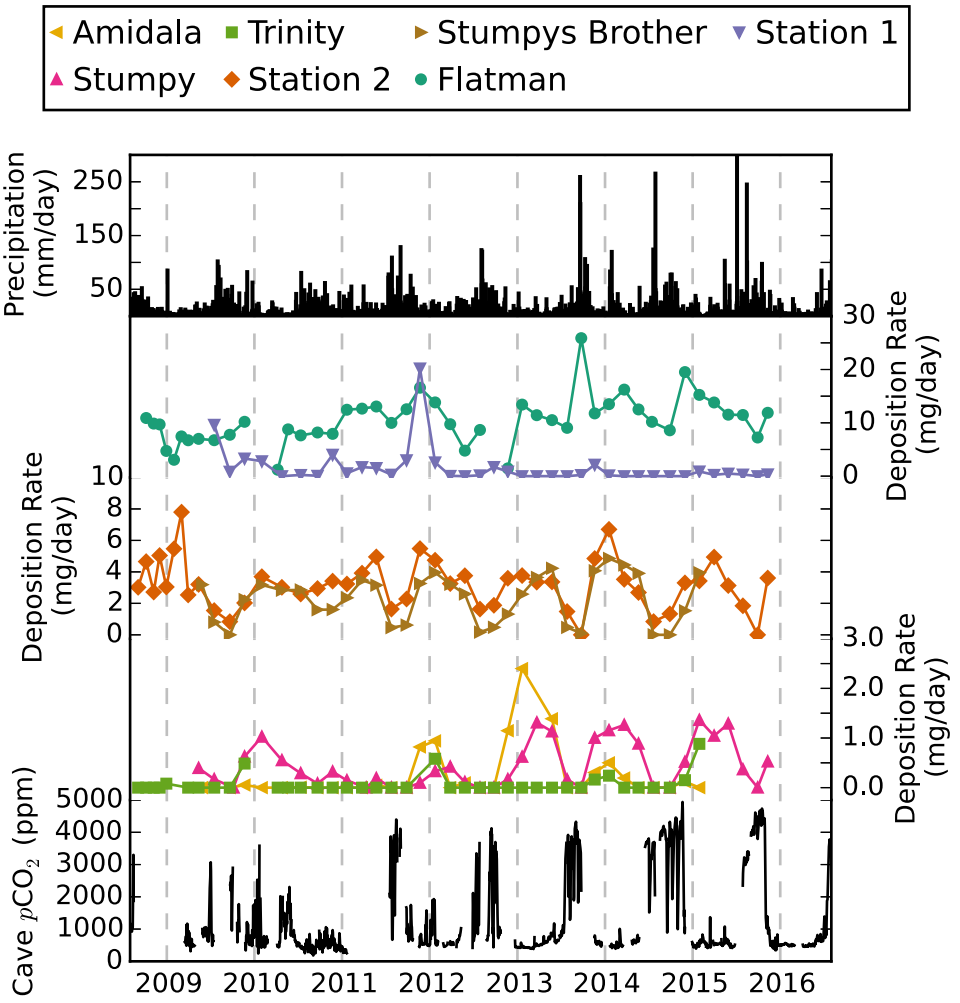

Figure 12. Daily average cave pCO_2, measured calcite depostion rate, and precipation amount. Calcite depostion rates at all seven drip sites are presented in three subplots with increasing depostion rates moving from bottom to top.

to reduce the initial concentration of dissolved carbonate species and calcium ion [*Dreybrodt and Scholz*, 2011], and in the zone of calcite precipitation low pCO_2 will increase in the amount of prior calcite precipitation [*Fairchild and Treble*, 2009]. The seasonality in drip water [Ca^{2+}] at some sites (Figure 7) suggests one or both mechanisms is occurring at Jinapsan Cave.

Figure 12 shows observed calcite deposition rates alongside cave pCO_2 and meteoric precipitation amount—the latter of which is closely tied to drip rate (Figure 6). Not shown here, drip water temperature is essentially uniform over the period of study. At all sites that display seasonality in calcite deposition rate, cessation of calcite deposition corresponds to intervals of high pCO_2 and high meteoric precipitation rate, suggesting that cave pCO_2 exerts strong control on the seasonality of cave calcite deposition rates. Seasonality in calcite deposition rate is evident at sites with the lowest drip rates, except for Amidala and Station 1, where deposition occurs only during periods of increased water availability. There is some seasonality in calcite deposition rate at Flatman, but the trend is not as distinct, which may indicate a relatively stronger influence of drip rate at this site.

Plates deployed at Trinity show evidence of dissolution, suggesting that the very high drip rate of the site drives net negative growth rates through erosion of the glass and potentially calcite redissolution. In a total of 42 plates deployed at Trinity, only 10 were recorded as weighing more when collected than before they were deployed, with the remaining 32 measured as weighing less following collection. Measured drip interval at Trinity is always < 2 s, with an average of 0.8 s. *Hansen et al.* [2013] showed that the time required for complete degassing of CO_2 from a 0.01 cm thin film is $\sim$2 s, and hypothesized that drip rates in this range

may result in dissolution of calcite on the stalagmite apex, making such samples disadvantageous for paleoclimate reconstruction.

As outlined in equations (1) and (2), speleothem calcite deposition rate is a function of both the degree of supersaturation of drip waters and the drip rate. Figure 8 shows the results of this model of stalagmite calcite deposition rate in time series, which appear to yield a poor representation of the observed calcite deposition rate. Excluding Trinity due to the evidence of redissolution, regression of modeled and measured calcite deposition rates yields an $r^2 = 0.38$. This result contrasts with other studies which have reported correlation coefficients ranging from 0.61–0.89 and have concluded that this model is able to reliably predict observed stalagmite calcite deposition rates [e.g., *Baker et al*., 1998, 2014; *Sherwin and Baldini*, 2011; *Casteel and Banner*, 2015]. The ability of the model to represent the observed seasonality in calcite deposition suggests that the deficiency is in the treatment of drip hydrology and the flow of water over the glass substrate.

Baker et al. [2014] demonstrated that film thickness on an infinite flat plane is much thicker than a film on a curved surface, with film thickness approaching 0.09 and 0.08 cm on smooth and etched flat surfaces respectively. In this study, care was taken to ensure that all plates were deployed with a slight incline, therefore the case of a completely flat plane is not applicable. However, *Hansen et al*. [2013] measured film thicknesses in excess of 0.01 cm, with a maximum measured thickness of 0.05 cm, on 1 m etched flat glass plates dipped 0.5°, and *Day and Henderson*, [2011] reported a zone of water pooling on the down-dipped end of a 7.2 cm glass plate inclined 12°. These results suggest that thick films and pooling may be the source of the model mismatch observed here.

4.3. Implications for Speleothem Paleoclimatology

Jinapsan Cave, Guam is characterized by strong seasonality in both precipitation amount and carbonate chemistry, which both exert control on calcite deposition rates. The results presented here show that deposition of calcite is biased toward the dry season in Jinapsan Cave, which potentially biases paleoclimate reconstructions. In particular, this seasonality in calcite deposition rates may contribute to the lack of coherency between stable isotope and trace element records at this site observed by *Partin et al*. [2012]. The primary driver of variability in speleothem calcite $\delta^{18}O$ is generally accepted to be variability in the $\delta^{18}O$ of meteoric precipitation. Drip water $\delta^{18}O$ at Jinapsan Cave is seasonally invariant or displays muted seasonality relative to $\delta^{18}O$ of precipitation due to the seasonality of recharge [*Jones and Banner*, 2003] and vadose zone mixing. Assuming constant water-calcite fractionation throughout the year, seasonality in calcite deposition rates would not be expected to affect the fidelity of the stalagmite calcite stable isotope record.

By contrast, the mechanisms that drive cessation of calcite deposition are also often the primary drivers of variability in speleothem trace element ratios that are interpreted as proxies of moisture conditions [*Fairchild and Treble*, 2009]. The lack of calcite deposition during the wet season in Jinapsan Cave will cause a bias in calcite trace element ratios toward dry season values. If speleothem calcite is not deposited during the wet season, the ability to distinguish changes in moisture conditions through speleothem calcite trace elements is limited. Instead, speleothem trace elements records at this coastal cave site may be primarily controlled by other processes, including sea spray [*Tremaine et al*., 2016].

5. Conclusions

The results of this 8 year monitoring study of Jinapsan Cave, Guam demonstrate the seasonal migration of the ITCZ modulates cave hydrology and cave atmospheric composition at this site. Of the seven drip sites monitored monthly, drip rate at five sites has seasonal variability that follows seasonal precipitation amount. Cave pCO_2 logged hourly shows cave pCO_2 varies seasonally between ~500 and 5000 ppm, which represents a much larger range of cave pCO_2 than previously reported in a tropical cave. We demonstrate that this seasonality cannot be explained by temperature-driven chimney effect airflow. Instead based on the coherence between cave pCO_2 and regional wind patterns, we argue for seasonal trade wind flow across the island as the dominant control on cave ventilation in Jinapsan Cave. This result highlights the importance of a variety of advective processes in karst, and demonstrates that advection can have important effects on cave pCO_2 and carbonate chemistry, even in tropical sites that have been thought to have more simple ventilation regimes [*James et al*., 2015].

We compare observed calcite deposition rates at Jinapsan Cave to the calcite deposition rate expected based on a model of stalagmite calcite precipitation rate. While the modeled values show seasonality in deposition rates, contrary to previous studies there is overall poor agreement between modeled and measured calcite deposition rates. We hypothesize that much of the model mismatch and disagreement with previous studies may be in the treatment of drip hydrology, and highlight the importance of further work on film thicknesses on both glass plate substrates used to collect calcite in cave monitoring programs and natural stalagmites.

Acknowledgments
Funding was provided by the NSF Paleo Perspectives on Climate Change Program (grant 1003700), NSF Geobiology and Low Temperature Geochemistry Program (grant 1452024), Pacific Island Climate Science Center, Guam Hydrologic Survey, Strategic Environmental Research and Development Program, and the Geology Foundation and Environmental Science Institute of the University of Texas at Austin. We thank Danko Taboroši and John and Joan Mylroie for their work mapping the cave, Christopher Maupin for his assistance with ICP-OES analyses, Nathan Miller for assistance with ICP-MS analyses, and Matt Covington and one anonymous reviewer for their helpful comments that significantly improved this manuscript. Thanks also to the many student and volunteer workers: Tomoko Bell, Vivianna Bendixson, Paul Bourke, Bekah Dougher, Jocelyn Emia, Scarlette Hsia, Walter Kelly, Maria Kottermair, Mark Moore, Rawlin Manzanilla, Blaz Miklavič, Leena Muller, Nathan Van Oort, Kara Posso, Ida Shalilian, Christine Simard, Erin Spaller-Miller, Daniel Superales, and Rachel Wright. Data and Python code are available for download at github.com/anoronha.

References

Atkinson, T. C. (1977), Carbon dioxide in the atmosphere of the unsaturated zone: An important control of groundwater hardness in limestones, *J. Hydrol.*, *35*, 111–123.

Baker, A., D. Genty, W. Dreybrodt, W. L. Barnes, N. J. Mockler, and J. Grapes (1998), Testing theoretically predicted stalagmite growth rate with recent annually laminated samples: Implications for past stalagmite deposition, *Geochim. Cosmochim. Acta*, *62*(3), 393–404.

Baker, A. J., D. P. Mattey, and J. U. L. Baldini (2014), Reconstructing modern stalagmite growth from cave monitoring, local meteorology, and experimental measurements of dripwater films, *Earth Planet. Sci. Lett.*, *392*, 239–249, doi:10.1016/j.epsl.2014.02.036.

Baldini, J. U. L. (2010), Cave atmosphere controls on stalagmite growth rate and palaeoclimate records, *Geol. Soc. Spec. Publ.*, *336*(1), 283–294, doi:10.1144/SP336.15.

Baldini, J. U. L., F. McDermott, D. L. Hoffmann, D. A. Richards, and N. Clipson (2008), Very high-frequency and seasonal cave atmosphere PCO_2 variability: Implications for stalagmite growth and oxygen isotope-based paleoclimate records, *Earth Planet. Sci. Lett.*, *272*(1–2), 118–129, doi:10.1016/j.epsl.2008.04.031.

Banner, J. L., A. Guilfoyle, E. W. James, L. A. Stern, and M. Musgrove (2007), Seasonal variations in modern speleothem calcite growth in central Texas, U.S.A., *J. Sediment. Res.*, *77*(8), 615–622, doi:10.2110/jsr.2007.065.

Benavente, J., I. Vadillo, F. Carrasco, A. Soler, C. Liñán, and F. Moral (2010), Air carbon dioxide contents in the vadose zone of a Mediterranean Karst, *Vadose Zone J.*, *9*(1), 126–136, doi:10.2136/vzj2009.0027.

Boch, R., C. Spötl, and S. Frisia (2011), Origin and palaeoenvironmental significance of lamination in stalagmites from Katerloch Cave, Austria, *Sedimentology*, *58*(2), 508–531, doi:10.1111/j.1365-3091.2010.01173.x.

Breecker, D. O., A. E. Payne, J. Quade, J. L. Banner, C. E. Ball, K. W. Meyer, and B. D. Cowan (2012), The sources and sinks of CO_2 in caves under mixed woodland and grassland vegetation, *Geochim. Cosmochim. Acta*, *96*, 230–246, doi:10.1016/j.gca.2012.08.023.

Cai, B., J. Zhu, F. Ban, and M. Tan (2011), Intra-annual variation of the calcite deposition rate of drip water in Shihua Cave, Beijing, China and its implications for palaeoclimatic reconstructions, *Boreas*, *40*(3), 525–535, doi:10.1111/j.1502-3885.2010.00201.x.

Casteel, R. C., and J. L. Banner (2015), Temperature-driven seasonal calcite growth and drip water trace element variations in a well-ventilated Texas cave: Implications for speleothem paleoclimate studies, *Chem. Geol.*, *392*, 43–58, doi:10.1016/j.chemgeo.2014.11.002.

Covington, M. D. (2015), The importance of advection for CO_2 dynamics in the karst critical zone: An approach from dimensional analysis, *Geol. Soc. Am. Spec. Pap.*, *516*, SPE516-09, doi:10.1130/2015.2516(09).

Covington, M. D., and M. Perne (2015), Consider a cylindrical cave: A physicist's view of cave and karst science, *Acta Carsolog.*, *44*(3), 363–380.

Day, C. C., and G. M. Henderson (2011), Oxygen isotopes in calcite grown under cave-analogue conditions, *Geochim. Cosmochim. Acta*, *75*(14), 3956–3972, doi:10.1016/j.gca.2011.04.026.

Dietzel, M., J. Tang, A. Leis, and S. J. Köhler (2009), Oxygen isotopic fractionation during inorganic calcite precipitation—Effects of temperature, precipitation rate and pH, *Chem. Geol.*, *268*(1–2), 107–115, doi:10.1016/j.chemgeo.2009.07.015.

Dreybrodt, W. (1988), *Processes in Karst Systems: Physics, Chemistry, and Geology*, Springer. http://link.springer.com/book/10.1007%2F978-3-642-83352-6.

Dreybrodt, W., and H. W. Franke (1987), Wachstumsgeschwindigkeiten und durchmesser von kerzenstalagmiten, *Die Höhle*, *38*(1), 1–6.

Dreybrodt, W., and D. Scholz (2011), Climatic dependence of stable carbon and oxygen isotope signals recorded in speleothems: From soil water to speleothem calcite, *Geochim. Cosmochim. Acta*, *75*(3), 734–752, doi:10.1016/j.gca.2010.11.002.

Dreybrodt, W., L. Eisenlohr, B. Madry, and S. Ringer (1997), Precipitation kinetics of calcite in the system $CaCO_3$—H_2O—CO_2: The conversion to CO2 by the slow process $H+ + HCO_3- \rightarrow CO_2 + H2_O$ as a rate limiting step, *Geochim. Cosmochim. Acta*, *61*(18), 3897–3904, doi:10.1016/S0016-7037(97)00201-9.

Duan, F., J. Wu, Y. Wang, R. L. Edwards, H. Cheng, X. Kong, and W. Zhang (2015), A 3000-yr annually laminated stalagmite record of the Last Glacial Maximum from Hulu Cave, China, *Quat. Res.*, *83*, 360–369, doi:10.1016/j.yqres.2015.01.003.

Faimon, J., M. B. Ličbinská, P. Zajíček, and O. E. Sracek (2012), Partial pressures of CO_2 in Epikarstic zone deduced from hydrogeochemistry of permanent drips, the Moravian Karst, Czech Republic [Delni Tlak CO_2 V Epikraški Coni, Kot Ga Razkrivajo Hidrokemične Raziskave Stalnih Vodnih Curkov], *Acta Carsolog.*, *41*(1), 47–57.

Fairchild, I. J., and P. C. Treble (2009), Trace elements in speleothems as recorders of environmental change, *Quat. Sci. Rev.*, *28*(5–6), 449–468, doi:10.1016/j.quascirev.2008.11.007.

Feng, W., J. L. Banner, A. L. Guilfoyle, M. Musgrove, and E. W. James (2012), Oxygen isotopic fractionation between drip water and speleothem calcite: A 10-year monitoring study, central Texas, USA, *Chem. Geol.*, *304 305–*, 53–67, doi:10.1016/j.chemgeo.2012.02.004.

Feng, W., R. C. Casteel, J. L. Banner, and A. Heinze-Fry (2014), Oxygen isotope variations in rainfall, drip-water and speleothem calcite from a well-ventilated cave in Texas, USA: Assessing a new speleothem temperature proxy, *Geochim. Cosmochim. Acta*, *127*, 233–250, doi:10.1016/j.gca.2013.11.039.

Frappier, A. B., D. Sahagian, S. J. Carpenter, L. A. González, and B. R. Frappier (2007), Stalagmite stable isotope record of recent tropical cyclone events, *Geology*, *35*(2), 111–114, doi:10.1130/G23145A.1.

Frisia, S., I. J. Fairchild, J. Fohlmeister, R. Miorandi, C. Spötl, and A. Borsato (2011), Carbon mass-balance modelling and carbon isotope exchange processes in dynamic caves, *Geochim. Cosmochim. Acta*, *75*(2), 380–400, doi:10.1016/j.gca.2010.10.021.

Gabitov, R. I., E. B. Watson, and A. Sadekov (2012), Oxygen isotope fractionation between calcite and fluid as a function of growth rate and temperature: An in situ study, *Chem. Geol.*, *306–307*, 92–102, doi:10.1016/j.chemgeo.2012.02.021.

Genty, D., A. Baker, and B. Vokal (2001), Instra- and inter-annual growth rate of modern stalagmites, *Chem. Geol.*, *176*(1–4), 191–212, doi:10.1016/S0009-2541(00)00399-5.

Hansen, M., W. Dreybrodt, and D. Scholz (2013), Chemical evolution of dissolved inorganic carbon species flowing in thin water films and its implications for (rapid) degassing of CO_2 during speleothem growth, *Geochim. Cosmochim. Acta*, *107*, 242–251, doi:10.1016/j.gca.2013.01.006.

James, E. W., J. L. Banner, and B. Hardt (2015), A global model for cave ventilation and seasonal bias in speleothem paleoclimate records, *Geochem. Geophys. Geosyst.*, *16*(4), 1044–1051, doi:10.1002/2014GC005658.

Jamieson, R. A., J. U. L. Baldini, A. B. Frappier, and W. Müller (2015), Volcanic ash fall events identified using principal component analysis of a high-resolution speleothem trace element dataset, *Earth Planet. Sci. Lett.*, *426*, 36–45, doi:10.1016/j.epsl.2015.06.014.

Johnson, K. R., C. Hu, N. Belshaw, and G. M. Henderson (2006), Seasonal trace-element and stable-isotope variations in a Chinese speleothem: The potential for high-resolution paleomonsoon reconstruction, *Earth Planet. Sci. Lett.*, *244*(1–2), 394–407, doi:10.1016/j.epsl.2006.01.064.

Jones, I. C., and J. L. Banner (2003), Estimating recharge thresholds in tropical karst island aquifers: Barbados, Puerto Rico and Guam, *J. Hydrol.*, *278*(1–4), 131–143, doi:10.1016/S0022-1694(03)00138-0.

Kalnay, E., et al. (1996), The NCEP/NCAR 40-year reanalysis project, *Bull. Am. Meteorol. Soc.*, *77*(3), 437–471, doi:10.1175/1520-0477.

Kubota, H., and B. Wang (2009), How much do tropical cyclones affect seasonal and interannual rainfall variability over the western North Pacific?, *J. Clim.*, *22*(20), 5495–5510, doi:10.1175/2009JCLI2646.1.

Lander, M. A., and C. P. Guard (2003), Creation of a 50-year rainfall database, annual rainfall climatology, and annual rainfall distribution map for Guam, *Tech. Rep. 102*, Water and Environ. Res. Inst. of the West. Pac., Mangilao, Guam.

Lander, M. A., J. W. Jenson, and C. Beausoliel (2001), Responses of well water levels on Northern Guam to variations of rainfall and sea level, *Tech. Rep. 94*, Water and Environ. Res. Inst. of the West. Pac., Mangilao, Guam.

Liu, Y., G. Tang, X. Ling, C. Hu, and X. Li (2015), Speleothem annual layers revealed by seasonal SIMS δ 18O measurements, *Sci. China Earth Sci.*, *58*(10), 1741–1747, doi:10.1007/s11430-015-5114-6.

Liu, Y.-H., G. M. Henderson, C. Hu, A. J. Mason, N. Charnley, K. R. Johnson, and S.-C. Xie (2013), Links between the East Asian monsoon and North Atlantic climate during the 8,200 year event, *Nat. Geosci.*, *6*(2), 117–120, doi:10.1038/ngeo1708.

Malhi, Y., D. D. Baldocchi, and P. G. Jarvis (1999), The carbon balance of tropical, temperate and boreal forests, *Plant Cell Environ.*, *22*, 715–740, doi:10.1046/j.1365-3040.1999.00453.x.

Mattey, D. P., D. Lowry, J. Duffet, R. Fisher, E. Hodge, and S. Frisia (2008), A 53 year seasonally resolved oxygen and carbon isotope record from a modern Gibraltar speleothem: Reconstructed drip water and relationship to local precipitation, *Earth Planet. Sci. Lett.*, *269*(1–2), 80–95, doi:10.1016/j.epsl.2008.01.051.

Mattey, D. P., I. J. Fairchild, T. C. Atkinson, J.-P. Latin, M. Ainsworth, and R. Durell (2010), Seasonal microclimate control of calcite fabrics, stable isotopes and trace elements in modern speleothem from St Michaels Cave, Gibraltar, *Geol. Soc. Spec. Publ.*, *336*(1), 323–344, doi:10.1144/SP336.17.

Maupin, C. R., J. W. Partin, C.-C. Shen, T. M. Quinn, K. Lin, F. W. Taylor, J. L. Banner, K. Thirumalai, and D. J. Sinclair (2013), Persistent decadal-scale rainfall variability in the tropical South Pacific Convergence Zone through the past six centuries, *Clim. Past Discuss.*, *9*(5), 5593–5625, doi:10.5194/cpd-9-5593-2013.

Mcgroddy, M., and W. L. Silver (2000), Variations in belowground carbon storage and soil CO_2 flux rates along a wet tropical climate gradient, *Biotropica*, *32*(4a), 614–624.

Menne, M. J., I. Durre, R. S. Vose, B. E. Gleason, T. G. Houston, M. J. Menne, I. Durre, R. S. Vose, B. E. Gleason, and T. G. Houston (2012), An overview of the global historical climatology network-daily database, *J. Atmos. Oceanic Technol.*, *29*(7), 897–910, doi:10.1175/JTECH-D-11-00103.1.

Miklavič, B. (2011), Formation of geomorphic features as a response to sea-level change at Ritidian Point, Guam, Mariana, MS thesis, Dep. of Geosci., Miss. State Univ., Starkville.

Moquet, J. S., et al. (2016), Calibration of speleothem δ18O records against hydroclimate instrumental records in Central Brazil, *Global Planet. Change*, *139*, 151–164, doi:10.1016/j.gloplacha.2016.02.001.

Motavalli, P. P., H. Discekici, and J. Kuhn (2000), The impact of land clearing and agricultural practices on soil organic C fractions and CO_2 efflux in the Northern Guam aquifer, *Agric. Ecosyst. Environ.*, *79*(1), 17–27, doi:10.1016/S0167-8809(99)00139-5.

Orland, I. J., Y. Burstyn, M. Bar-Matthews, R. Kozdon, A. Ayalon, A. Matthews, and J. W. Valley (2014), Seasonal climate signals (1990–2008) in a modern Soreq Cave stalagmite as revealed by high-resolution geochemical analysis, *Chem. Geol.*, *363*, 322–333, doi:10.1016/j.chemgeo.2013.11.011.

Partin, J. W., et al. (2012), Relationship between modern rainfall variability, cave dripwater, and stalagmite geochemistry in Guam, USA, *Geochem. Geophys. Geosyst.*, *13*, Q03013, doi:10.1029/2011GC003930.

Partin, J. W., et al. (2013a), Multidecadal rainfall variability in South Pacific Convergence Zone as revealed by stalagmite geochemistry, *Geology*, *41*(11), 1143–1146, doi:10.1130/G34718.1.

Partin, J. W., K. M. Cobb, J. F. Adkins, A. A. Tuen, and B. Clark (2013b), Trace metal and carbon isotopic variations in cave dripwater and stalagmite geochemistry from northern Borneo, *Geochem. Geophys. Geosyst.*, *14*(9), 3567–3585, doi:10.1002/ggge.20215.

Peyraube, N., R. Lastennet, A. Denis, and P. Malaurent (2013), Estimation of epikarst air PCO_2 using measurements of water δ13CTDIC, cave air PCO_2 and d13CCO_2, *Geochim. Cosmochim. Acta*, *118*, 1–17, doi:10.1016/j.gca.2013.03.046.

Pu, J., A. Wang, L. Shen, J. Yin, D. Yuan, and H. Zhao (2015), Factors controlling the growth rate, carbon and oxygen isotope variation in modern calcite precipitation in a subtropical cave, Southwest China, *J. Asian Earth Sci.*, *119*, 167–178, doi:10.1016/j.jseaes.2015.12.010.

Rasbury, M., and P. Aharon (2006), ENSO-controlled rainfall variability records archived in tropical stalagmites from the mid-ocean island of Niue, South Pacific, *Geochem. Geophys. Geosyst.*, *7*, Q07010, doi:10.1029/2005GC001232.

Rasmussen, J. B. T., V. J. Polyak, and Y. Asmerom (2006), Evidence for Pacific-modulated precipitation variability during the late Holocene from the southwestern USA, *Geophys. Res. Lett.*, *33*, L08701, doi:10.1029/2006GL025714.

Ridley, H. E., et al. (2015a), Aerosol forcing of the position of the intertropical convergence zone since ad 1550, *Nat. Geosci.*, *8*(3), 195–200, doi:10.1038/ngeo2353.

Ridley, H. E., J. U. L. Baldini, K. Prufer, I. Walczak, and S. Breitenbach (2015b), High-resolution monitoring of Yok Balum Cave, Belize: An investigation of seasonal ventilation regimes and the atmospheric and drip-flow response to a local earthquake, *J. Cave Karst Stud.*, *77*(3), 183–199, doi:10.4311/2014ES0117.

Riechelmann, D. F. C., J. Fohlmeister, R. Tjallingii, K. P. Jochum, D. K. Richter, G.-J. A. Brummer, and D. Scholz (2016), Detection and origin of different types of annual laminae in recent stalagmites from Zoolithencave, southern Germany: Evaluation of the potential for

quantitative reconstruction of past precipitation variability, *Clim. Past Discuss.*, 1–42, doi:10.5194/cp-2016-18. http://www.clim-past-discuss.net/cp-2016-18/.

Romanov, D., G. Kaufmann, and W. Dreybrodt (2008a), Modeling stalagmite growth by first principles of chemistry and physics of calcite precipitation, *Geochim. Cosmochim. Acta*, *72*(2), 423–437, doi:10.1016/j.gca.2007.09.038.

Romanov, D., G. Kaufmann, and W. Dreybrodt (2008b), $\delta^{13}C$ profiles along growth layers of stalagmites: Comparing theoretical and experimental results, *Geochim. Cosmochim. Acta*, *72*(2), 438–448, doi:10.1016/j.gca.2007.09.039.

Ruan, J., and C. Hu (2010), Seasonal variations and environmental controls on stalagmite calcite crystal growth in Heshang Cave, central China, *Chin. Sci. Bull.*, *55*(34), 3929–3935, doi:10.1007/s11434-010-4193-1.

Sánchez-Cañete, E. P., P. Serrano-Ortiz, F. Domingo Poveda, and A. S. Kowalski (2013), Cave ventilation is influenced by variations in the CO_2-dependent virtual temperature, *Int. J. Speleol.*, *42*(1), 1–8.

Sánchez-Cañete, E. P., C. Oyonarte, P. Serrano-Ortiz, J. Curiel Yuste, O. Pérez-Priego, F. Domingo, and A. S. Kowalski (2016), Winds induce CO_2 exchange with the atmosphere and vadose zone transport in a karstic ecosystem, *J. Geophys. Res. Biogeosci.*, *121*, 2049–2063, doi:10.1002/2016JG003500.

Schrag, D. P. (1999), Rapid analysis of high-precision Sr/Ca ratios in corals and other marine carbonates, *Paleoceanography*, *14*(2), 97–102.

Sherwin, C. M., and J. U. L. Baldini (2011), Cave air and hydrological controls on prior calcite precipitation and stalagmite growth rates: Implications for palaeoclimate reconstructions using speleothems, *Geochim. Cosmochim. Acta*, *75*(14), 3915–3929, doi:10.1016/j.gca.2011.04.020.

Sinclair, D. J., J. L. Banner, F. W. Taylor, J. W. Partin, J. Jenson, J. E. Mylroie, E. Goddard, T. Quinn, J. Jocson, and B. Miklavič (2012), Magnesium and strontium systematics in tropical speleothems from the Western Pacific, *Chem. Geol.*, *294 295–*, 1–17, doi:10.1016/j.chemgeo.2011.10.008.

Smith, A., N. Lott, R. Vose, A. Smith, N. Lott, and R. Vose (2011), The integrated surface database: recent developments and partnerships, *Bull. Am. Meteorol. Soc.*, *92*(6), 704–708, doi:10.1175/2011BAMS3015.1.

Stoll, H. M., A. Mendez-Vicente, S. Gonzalez-Lemos, A. Moreno, I. Cacho, H. Cheng, and R. L. Edwards (2015), Interpretation of orbital scale variability in mid-latitude speleothem δ18O: Significance of growth rate controlled kinetic fractionation effects, *Quat. Sci. Rev.*, *127*, 215–228, doi:10.1016/j.quascirev.2015.08.025.

Tan, L., L. Yi, Y. Cai, C.-C. Shen, H. Cheng, and Z. An (2013), Quantitative temperature reconstruction based on growth rate of annually-layered stalagmite: A case study from central China, *Quat. Sci. Rev.*, *72*, 137–145, doi:10.1016/j.quascirev.2013.04.022.

Tan, M., A. Baker, D. Genty, C. L. Smith, J. Esper, and B. Cai (2006), Applications of stalagmite laminae to paleoclimate reconstructions: Comparison with dendrochronology/climatology, *Quat. Sci. Rev.*, *25*(17–18), 2103–2117, doi:10.1016/j.quascirev.2006.01.034.

Tremaine, D. M., P. N. Froelich, and Y. Wang (2011), Speleothem calcite farmed in situ: Modern calibration of $\delta^{18}O$ and $\delta^{13}C$ paleoclimate proxies in a continuously-monitored natural cave system, *Geochim. Cosmochim. Acta*, *75*(17), 4929–4950, doi:10.1016/j.gca.2011.06.005.

Tremaine, D. M., D. J. Sinclair, H. M. Stoll, M. Lagerström, C. P. Carvajal, and R. M. Sherrell (2016), A two-year automated dripwater chemistry study in a remote cave in the tropical south Pacific: Using [Cl-] as a conservative tracer for seasalt contribution of major cations, *Geochim. Cosmochim. Acta*, *184*, 289–310, doi:10.1016/j.gca.2016.03.029.

Van Rampelbergh, M., S. Verheyden, M. Allan, Y. Quinif, H. Cheng, L. R. Edwards, E. Keppens, and P. Claeys (2015), A 500-year seasonally resolved $\delta^{18}O$ and $\delta^{13}C$, layer thickness and calcite aspect record from a speleothem deposited in the Han-sur-Lesse cave, Belgium, *Clim. Past*, *11*(6), 789–802, doi:10.5194/cp-11-789-2015.

Watkins, J. M., J. D. Hunt, F. J. Ryerson, and D. J. DePaolo (2014), The influence of temperature, pH, and growth rate on the $\delta^{18}O$ composition of inorganically precipitated calcite, *Earth Planet. Sci. Lett.*, *404*, 332–343, doi:10.1016/j.epsl.2014.07.036.

Watson, E. B. (2004), A conceptual model for near-surface kinetic controls on the trace-element and stable isotope composition of abiogenic calcite crystals, *Geochim. Cosmochim. Acta*, *68*(7), 1473–1488, doi:10.1016/j.gca.2003.10.003.

Wigley, T. M. L., and M. C. Brown (1976), The Physics of Caves, in *The Science of Speleology*, edited by T. D. Ford and C. H. D. Cullingford, pp. 329–358, Academic, London, U. K.

Wong, C. I., and D. O. Breecker (2015), Advancements in the use of speleothems as climate archives, *Quat. Sci. Rev.*, *127*, 1–18, doi:10.1016/j.quascirev.2015.07.019.

Wong, C. I., J. L. Banner, and M. Musgrove (2011), Seasonal dripwater Mg/Ca and Sr/Ca variations driven by cave ventilation: Implications for and modeling of speleothem paleoclimate records, *Geochim. Cosmochim. Acta*, *75*(12), 3514–3529, doi:10.1016/j.gca.2011.03.025.

Wu, J., X. Shao, X. Kong, and Y. Wang (2006), Imprint of solar activity on Nanjing stalagmite annual layer thickness sequence during the Last Glacial Maximum, *Chin. Sci. Bull.*, *51*(4), 441–447, doi:10.1007/s11434-006-0441-9.

Wynn, P. M., I. J. Fairchild, S. Frisia, C. Spötl, A. Baker, and A. Borsato (2010), High-resolution sulphur isotope analysis of speleothem carbonate by secondary ionisation mass spectrometry, *Chem. Geol.*, *271*(3–4), 101–107, doi:10.1016/j.chemgeo.2010.01.001.

Xie, P., and P. A. Arkin (1996), Analyses of global monthly precipitation using gauge observations, satellite estimates, and numerical model predictions, *J. Clim.*, *9*(4), 840–858, doi:10.1175/1520-0442(1996)009<0840:AOGMPU>2.0.CO;2.